World Scientific
www.worldscientific.com

Bridge Damping Formula Based on Instantaneous Amplitudes of Vehicle's Front and Rear Contact Responses by Hilbert Transform

Y. B. Yang ⓘ*,†,‡,¶, M. Yang*,†, Ding-Han Liu§,
Y. H. Liu ⓘ*,† and H. Xu ⓘ*,†,∥

*School of Civil Engineering, Chongqing University
Chongqing 400045, P. R. China

†MOE Key Laboratory of New Technology for
Construction of Cities in Mountain Area
Chongqing University, Chongqing, P. R. China

‡School of Civil Engineering and Architecture
Chongqing University of Science and Technology
Chongqing 401331, P. R. China

§School of Civil Engineering, Tsinghua University
Beijing 100084, P. R. China

¶ybyang@cqu.edu.cn
∥hxu@cqu.edu.cn

In this paper, a simple formula is derived for the modal damping ratio of the bridge using the correlation between the instantaneous amplitudes of the related front and rear contact responses of a two-axle test vehicle by the Hilbert transform (HT). To start, closed-form solutions were derived for the dynamic response of the damped bridge and vehicle-bridge contact responses. Next, the HT was employed to generate the instantaneous amplitudes of the two contact points. Based on their correlation, a simple formula is derived for the bridge damping ratio. Finally, the reliability of the derived formula was verified in the numerical study. It was demonstrated that the proposed formula can be successfully used to determine the first bridge damping ratio, even in the presence of rough pavement, but with the aid of random traffic.

1. Introduction

Modal parameters such as frequencies, damping ratios, and mode shapes are the key properties that can reflect the health state of a bridge. To assess the health

---

∥Corresponding author.

condition of the bridge, structural health monitoring (SHM) has frequently been employed.[1,2] Conventionally, the modal parameters of bridges are identified by the vibration sensors directly deployed on the bridge of concern. Such an approach is known as the direct approach, which suffers from the drawbacks of high cost in installation and maintenance of the monitoring system, huge amount of data not well digested, and short life-span of the sensors deployed with respect to the bridge to be monitored, among others. Alternatively, the vehicle scanning method (VSM), originally known as the indirect method, was proposed by Yang *et al.*[3] for identifying the properties of a bridge from the data recorded by a test vehicle during its passage. Over the past two decades, the research on VSM has grown rapidly and globally,[4] including those on identification of bridge frequencies,[3,5–7] mode shapes,[8–11] and damping ratios.[12–15]

To effectively extract the bridge frequencies from the test vehicle response, the empirical mode decomposition (EMD),[16,17] generalized pattern search algorithm,[18] cross-spectral density function,[19] and second-order synchrosqueezing transform[20] were adopted. In addition, time-frequency analysis techniques have also been adopted for bridge modal parameter identification, including the short-time Fourier transform,[5,9] wavelet transform (WT),[11,21,22] synchroextracting transform,[23] etc. However, the vehicle response has been criticized for the fact that the frequencies of the test vehicle itself may appear as outstanding peaks in the vehicle spectra, thereby rendering the bridge frequencies invisible. To tackle this issue, techniques such as the particle filter approach,[24] vehicle-bridge contact response,[7,25] matrix completion method[26,27] vehicle's frequency response function (FRF),[10] and Kalman filter[28] have been employed. The contact response will be adopted in this paper for its effectiveness in suppressing the vehicle frequencies.

In contrast, the damping ratio, another important property of the bridge, has not been very well studied using the VSM. In the literature, the following techniques have been adopted: six-step algorithm,[12] truck-trailer system,[13] laser sensors,[14] and random-decrement technique (RDT).[15] For a two-axle test vehicle, the front and rear wheels may move over the same paths on the bridge, but differ by a phase shift. In previous studies, the correlation between the front and rear contact points of the test vehicle was not well utilized to determine the damping ratio of bridges. In this technical note, a simple formula will be derived for the modal damping ratio of the bridge using the correlation between the instantaneous amplitudes of the related front and rear contact responses of a two-axle test vehicle by the Hilbert transform (HT). The reliability of the proposed formula for determining the bridge damping ratio will be verified by the finite element method (FEM), and also demonstrated in the applications.

2. Theoretical Formulation of the Problem

In the theoretical formulation, the vehicle-bridge interaction (VBI) model adopted is a simply supported beam subjected to a two-axle test vehicle moving at speed v. As shown in Fig. 1, the test vehicle is modeled as a two degrees-of-freedom (DOF) system, consisting of a rigid beam (car body) of mass m_v and mass moment of inertia J_v, and supported by two spring-dashpot units, i.e. axles, of stiffnesses (k_{v1}, k_{v2}) and damping coefficients (c_{v1}, c_{v2}). The subscript ($j = 1$ and 2) denotes the front and rear axles, respectively. The distance between the two axles is d, and the distance of the jth axle to the vehicle's center of gravity is denoted by d_j. The equations for the vertical and rotational motions of the two-axle vehicle moving at speed v over the beam are

$$m_v \ddot{y}_v(t) + c_{v1}[\dot{y}_v(t) + d_1\dot{\theta}_v(t) - \dot{u}_{c1}(t)] + c_{v2}[\dot{y}_v(t) - d_2\dot{\theta}_v(t) - \dot{u}_{c2}(t)]$$

$$+ k_{v1}[y_v(t) + d_1\theta_v(t) - u_{c1}(t)] + k_{v2}[y_v(t) - d_2\theta_v(t) - u_{c2}(t)] = 0, \tag{1a}$$

$$J_v \ddot{\theta}_v(t) + c_{v1}d_1[\dot{y}_v(t) + d_1\dot{\theta}_v(t) - \dot{u}_{c1}(t)] - c_{v2}d_2[\dot{y}_v(t) - d_2\dot{\theta}_v(t) - \dot{u}_{c2}(t)]$$

$$+ k_{v1}d_1[y_v(t) + d_1\theta_v(t) - u_{c1}(t)] - k_{v2}d_2[y_v(t) - d_2\theta_v(t) - u_{c2}(t)] = 0. \tag{1b}$$

Here, $y_v(t)$ and $\theta_v(t)$ are the vertical displacement and rotational angle, respectively, of the mass center of vehicle body; u is the vertical displacement of the beam; $u_{cj}(t)$ is the contact displacement of the beam, i.e. $u_{cj}(t) = u(xt)|_{x=v(t-t_j)}$ with $t_j = (j-1)d/v$ denoting the entry time of the front and rear axles on the beam; and dot ($\bullet$) denotes the time derivative.
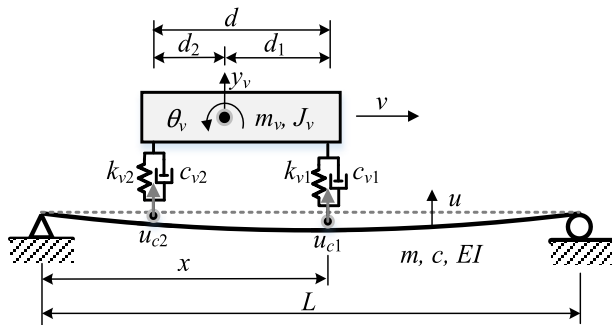

Fig. 1. A two-axle test vehicle travelling over a beam.

For the sake of deriving closed-form solution, the bridge is modeled as a simply supported beam of the Bernoulli–Euler type of span length L, elastic modulus E, moment of inertia I, damping coefficient c, and per-unit-length mass m. The equation of motion for the beam under the moving test vehicle is

$$m\ddot{u} + c\dot{u} + EIu'''' = F(t), \tag{2}$$

where prime ($'$) denotes the spatial derivative. In practice, the vehicle mass is very small relative to the bridge mass. By assuming the vehicle mass m_v to be much less than the bridge mass mL (i.e. $m_v \ll$ mL), the vehicle's action on the bridge can be simplified as two discrete moving loads $p_j (j = 1, 2)$, neglecting the dynamic interaction effect[4,29]

$$F(t) = \sum_{j=1,2} p_j \delta[x - v(t - t_j)][H(t - t_j) - H(t - t_j - T)], \tag{3}$$

where $\delta(\ )$ and $H(\ )$ denote the delta and unit step functions, respectively, and $p_j = (d - d_j)m_v g/d$ the axle loads, $T = L/v$ the travel time, and g the acceleration of gravity.

By the method of modal superposition,[30] the displacement of the beam can be obtained:

$$u(x,t) = \sum_n \sum_{i=1,2} \Delta_{\text{stn},i} \left\{ \begin{bmatrix} A_{bD,n} \cos(\omega_{bD,n}(t - t_i)) \\ + B_{bD,n} \sin(\omega_{bD,n}(t - t_i)) \end{bmatrix} e^{-\xi_{b,n}\omega_{b,n}(t-t_i)} \\ + A_{d,n} \cos(\omega_{d,n}(t - t_i)) + B_{d,n} \sin(\omega_{d,n}(t - t_i)) \right\}$$
$$\times \begin{bmatrix} H(t - t_i) \\ -H(t - t_i - T) \end{bmatrix} \sin \frac{n\pi x}{L}, \tag{4}$$

where for the nth mode of the beam, subscript i (= 1, 2) denotes the items to be summed over, $\Delta_{\text{stn},j}$ is the static deflection, $\xi_{b,n}$ the damping ratio, $\omega_{b,n}$ the natural frequency, $\omega_{bD,n}$ the damped frequency, and $\omega_{d,n}$ the driving frequency,

$$\Delta_{\text{stn},j} = \frac{-2p_j L^3}{n^4 \pi^4 EI}, \quad \xi_{b,n} = \frac{c}{2m\omega_{b,n}}, \tag{5a,b}$$

$$\omega_{b,n} = \frac{n^2\pi^2}{L^2}\sqrt{\frac{EI}{m}}, \quad \omega_{bD,n} = \omega_{b,n}\sqrt{1 - \xi_{b,n}^2}, \quad \omega_{d,n} = \frac{n\pi v}{L} \tag{6a-c}$$

and the coefficients are

$$A_{d,n} = \frac{-2\xi_{b,n}S_n}{(1 - S_n^2)^2 + (2\xi_{b,n}S_n)^2}, \quad B_{d,n} = \frac{(1 - S_n^2)}{(1 - S_n^2)^2 + (2\xi_{b,n}S_n)^2}, \tag{7a,b}$$

$$A_{bD,n} = -A_{d,n}, \quad B_{bD,n} = -\frac{\xi_{b,n}\omega_{b,n}A_{d,n} + \omega_{d,n}B_{d,n}}{\omega_{bD,n}}, \tag{7c,d}$$

with the speed parameter S_n,

$$S_n = \frac{n\pi v}{L\omega_{b,n}}. \tag{8}$$

By letting $x = v(t - t_j)$, the contact displacement of the beam $u_{cj}(t)$ for the jth axle can be obtained,

$$u_{cj}(t) = \sum_n \sum_{i=1,2} \Delta_{\text{stn},i} \left\{ \begin{bmatrix} A_{bD,n} \cos(\omega_{bD,n}(t - t_i)) \\ +B_{bD,n} \sin(\omega_{bD,n}(t - t_i)) \end{bmatrix} e^{-\xi_{b,n}\omega_{b,n}(t-t_i)} \\ +A_{d,n} \cos(\omega_{d,n}(t - t_i)) + B_{d,n} \sin(\omega_{d,n}(t - t_i)) \right\}$$

$$\times \begin{bmatrix} H(t - t_i) \\ -H(t - t_i - T) \end{bmatrix} \sin \frac{n\pi v(t - t_j)}{L}. \tag{9}$$

Theoretically, one can twice differentiate Eq. (9) to obtain the contact accelerations $\ddot{u}_{cj}(t)$, which however are not achievable in practice. Instead, they can be back-calculated from the measured vehicle's responses $\ddot{y}_v(t)$ and $\ddot{\theta}_v(t)$ using the equilibrium equations of the test vehicle in Eqs. (1a) and (1b). The formula so derived for the contact accelerations is Ref. 31.

$$\ddot{u}_{cj}(t) = \frac{1}{c_{vj}} e^{\frac{-k_{vj}}{c_{vj}}t} \int_0^t G_j(\tau) e^{\frac{k_{vj}}{c_{vj}}\tau} d\tau, \quad j = 1, 2, \tag{10}$$

where

$$G_1(t) = \left(\frac{d_2 m_v}{d}\right) \frac{d^2 \ddot{y}_v(t)}{dt^2} + \left(\frac{J_v}{d}\right) \frac{d^2 \ddot{\theta}_v(t)}{dt^2} + k_{v1}[\ddot{y}_v(t) + d_1 \ddot{\theta}_v(t)]$$

$$+ c_{v1} \left[\frac{d\ddot{y}_v(t)}{dt} + d_1 \frac{d\ddot{\theta}_v(t)}{dt} \right], \tag{11a}$$

$$G_2(t) = \left(\frac{d_1 m_v}{d}\right) \frac{d^2 \ddot{y}_v(t)}{dt^2} - \left(\frac{J_v}{d}\right) \frac{d^2 \ddot{\theta}_v(t)}{dt^2} + k_{v2}[\ddot{y}_v(t) - d_2 \ddot{\theta}_v(t)]$$

$$+ c_{v2} \left[\frac{d\ddot{y}_v(t)}{dt} - d_2 \frac{d\ddot{\theta}_v(t)}{dt} \right]. \tag{11b}$$

As can be seen, once the vehicle's vertical and rotational accelerations, $\ddot{y}_v(t)$ and $\ddot{\theta}_v(t)$, are made available, in addition to the vehicle properties, the term $G_j(t)$ can be obtained from Eq. (11a, 11b). Subsequently, the contact accelerations $\ddot{u}_{cj}(t)$ can be calculated by Eq. (10). The detailed derivation of Eq. (10) is available in Ref. 31.

3. Determination of Bridge Damping Ratio

In this section, the HT will be employed to extract the bridge damping ratio from the correlation between the front and rear contact responses of the two-axle vehicle. In this regard, the nth component response of the bridge is first filtered out from the two contact responses by the bandpass filter or mode decomposition technique.[31]

In this paper, only the case with the two wheels of the test vehicle *simultaneously* acting on the beam will be considered. In other words, no consideration will be made for the cases with the front wheel entering or the rear wheel departing from the beam. Theoretically, the nth component response of acceleration of the beam can be obtained from the contact displacement in Eq. (9). Since the driving frequency $n\pi v/L$ is much smaller than the damped bridge frequency $\omega_{bD,n}$, the terms $\omega_{brD,n}$ and $\omega_{blD,n}$ (i.e. $\omega_{bD,n} \pm n\pi v/L$) can be approximated as $\omega_{bD,n}$. Hence, the nth component response for the jth ($j = 1, 2$) contact responses can be obtained:

$$\ddot{u}_{cj,n}(t) = e^{-\xi_{b,n}\omega_{b,n}t} \sum_{i=1,2} \frac{\Delta_{stn,i}}{2} e^{\xi_{b,n}\omega_{b,n}t_i}$$

$$\times \begin{bmatrix} C_{b,n}\sin\left(\omega_{brD,n}t - \omega_{bD,n}t_i - \dfrac{n\pi vt_j}{L}\right) \\[2mm] -D_{b,n}\cos\left(\omega_{brD,n}t - \omega_{bD,n}t_i - \dfrac{n\pi vt_j}{L}\right) \\[2mm] -C_{b,n}\sin\left(\omega_{blD,n}t - \omega_{bD,n}t_i + \dfrac{n\pi vt_j}{L}\right) \\[2mm] +D_{b,n}\cos\left(\omega_{blD,n}t - \omega_{bD,n}t_i + \dfrac{n\pi vt_j}{L}\right) \end{bmatrix}, \qquad (12)$$

where

$$C_{b,n} = \xi_{b,n}^2\omega_{b,n}^2 A_{bD,n} - \omega_{bD,n}^2 A_{bD,n} - 2\xi_{b,n}\omega_{b,n}\omega_{bD,n}B_{bD,n}, \qquad (13a)$$

$$D_{b,n} = \xi_{b,n}^2\omega_{b,n}^2 B_{bD,n} - \omega_{bD,n}^2 B_{bD,n} + 2\xi_{b,n}\omega_{b,n}\omega_{bD,n}A_{bD,n}. \qquad (13b)$$

The transformed pair of Eq. (12) by the HT can be obtained as[33]

$$H[\ddot{u}_{cj,n}(t)] = e^{-\xi_{b,n}\omega_{b,n}t} \sum_{i=1,2} \frac{\Delta_{stn,i}}{2} e^{\xi_{b,n}\omega_{b,n}t_i}$$

$$\times \begin{bmatrix} -C_{b,n}\cos\left(\omega_{brD,n}t - \omega_{bD,n}t_i - \dfrac{n\pi vt_j}{L}\right) \\[2mm] -D_{b,n}\sin\left(\omega_{brD,n}t - \omega_{bD,n}t_i - \dfrac{n\pi vt_j}{L}\right) \\[2mm] +C_{b,n}\cos\left(\omega_{blD,n}t - \omega_{bD,n}t_i + \dfrac{n\pi vt_j}{L}\right) \\[2mm] +D_{b,n}\sin\left(\omega_{blD,n}t - \omega_{bD,n}t_i + \dfrac{n\pi vt_j}{L}\right) \end{bmatrix}. \qquad (14)$$

Hence, the instantaneous amplitude of the nth component response of the beam is

$$
A_{cj}(t) = \sqrt{(\ddot{u}_{cj,n})^2 + [H(\ddot{u}_{cj,n})]^2}
$$

$$
= e^{-\xi_{b,n}\omega_{b,n}t}\sqrt{(C_{b,n}^2 + D_{b,n}^2)\left[\begin{array}{c} 2\Delta_{\mathrm{stn},1}\Delta_{\mathrm{stn},2}e^{\xi_{b,n}\omega_{b,n}t_2}\cos(\omega_{bD,n}t_2) \\ + \sum\limits_{i=1,2}\Delta_{\mathrm{stn},i}^2 e^{2\xi_{b,n}\omega_{b,n}t_i} \end{array}\right]}
$$

$$
\times \sin\left[\frac{n\pi v(t - t_j)}{L}\right], \tag{15}
$$

where $\sin[n\pi v(t - t_j)/L]$ $j = 1, 2)$ represents the mode shape of the beam. From the front and rear contact responses, the instantaneous amplitudes of the nth component responses of the beam considering the damping effect of the beam are

$$
A_{c1}(t) = e^{-\xi_{b,n}\omega_{b,n}t}\sqrt{(C_{b,n}^2 + D_{b,n}^2)\left[\begin{array}{c} 2\Delta_{stn,1}\Delta_{stn,2}e^{\xi_{b,n}\omega_{b,n}t_2}\cos(\omega_{bD,n}t_2) \\ + \sum\limits_{i=1,2}\Delta_{stn,i}^2 e^{2\xi_{b,n}\omega_{b,n}t_i} \end{array}\right]}
$$

$$
\times \sin\left(\frac{n\pi vt}{L}\right), \tag{16a}
$$

$$
A_{c2}(t + t_2) = e^{-\xi_{b,n}\omega_{b,n}(t+t_2)}\sqrt{(C_{b,n}^2 + D_{b,n}^2)\left[\begin{array}{c} 2\Delta_{stn,1}\Delta_{stn,2}e^{\xi_{b,n}\omega_{b,n}t_2}\cos(\omega_{bD,n}t_2) \\ + \sum\limits_{i=1,2}\Delta_{stn,i}^2 e^{2\xi_{b,n}\omega_{b,n}t_i} \end{array}\right]}
$$

$$
\times \sin\left(\frac{n\pi vt}{L}\right). \tag{16b}
$$

By using the correlation between the instantaneous amplitudes of the nth component responses of the two contact responses in Eqs. (16a) and (16b), one obtains

$$
\frac{A_{c2}(t + t_2)}{A_{c1}(t)} = e^{-\xi_{b,n}\omega_{b,n}t_2}. \tag{17}
$$

It follows that the damping ratio for the nth mode is

$$
\xi_{b,n} = \frac{\ln\left[\frac{A_{c2}(t+t_2)}{A_{c1}(t)}\right]}{-\omega_{b,n}t_2}. \tag{18}
$$

The preceding equation enables us to compute the nth damping ratio $\xi_{b,n}$ of the beam in an easy way for the following reasons: The amplitudes $A_{c1}(t)$ and $A_{c2}(t+t_2)$ can be calculated by applying the HT to the nth component responses filtered out from the front and rear contact responses; the bridge frequency $\omega_{b,n}$ is available from the contact or vehicle spectra; and the entry time of the rear axle $t_2(= d/v)$ is a constant. Numerical examples will be presented below to demonstrate the application of the simple formula derived in Eq. (18).

4. Numerical Verification

4.1. *Verification of analytical solution*

The properties of the two-axle test vehicle and bridge adopted for the numerical analysis have been listed in Table 1, which have been typically used in previous studies to verify the accuracy of the analytical solutions.[7,31] For the bridge, the moment of inertia and mass per unit length adopted in Table 1 are close to those of a concrete I girder contained in a real bridge.[32] Such a bridge is adopted herein merely to demonstrate the application of the proposed method. Accordingly, the vertical and rotational frequencies computed of the test vehicle are $f_v = 4.35\,\text{Hz}$ and $f_r = 7.66\,\text{Hz}$[31] and the first two bridge frequencies from Eq. (6b) are $f_{bD,1} = 2.64\,\text{Hz}$ and $f_{bD,2} = 10.57\,\text{Hz}$, with the cyclic frequency $f = \omega/(2\pi)$.

The two-axle test vehicle is an extension of the single-axle vehicle used in Refs. 3 and 32, but can self-stand (unlike the single-axle test vehicle). It is not self powered, but needs to be towed by a tractor during the test. To achieve higher detectability for bridge frequencies from the vehicle response, the vehicle frequency is designed to be larger than the first bridge frequency,[7] as was done herein. Moreover, the bouncing effect of the two-axle test vehicle has been considered in the calculation of the contact responses in Eq. (10).

To verify the accuracy of the analytical solutions, pavement roughness is temporarily ignored. In addition, to evaluate the effect of multi-mode contribution, the observation point of the bridge is taken at 12 m from the left end. For the test vehicle moving at $v = 5\,\text{m/s}$ (18 km/h), the acceleration responses of the bridge calculated analytically and by the FEM have been plotted in Fig. 2(a), along with the acceleration spectra in Fig. 2(b). Evidently, the analytical solutions agree excellently with the FEM ones in both the time and frequency domains. This is a justification of the assumptions previously made in deriving the analytical solutions. To be specific, the first two bridge frequencies identified by the FEM in Fig. 2(b) are $f_{bD,1} = 2.67\,\text{Hz}$

Table 1. Vehicle and bridge properties.[31]

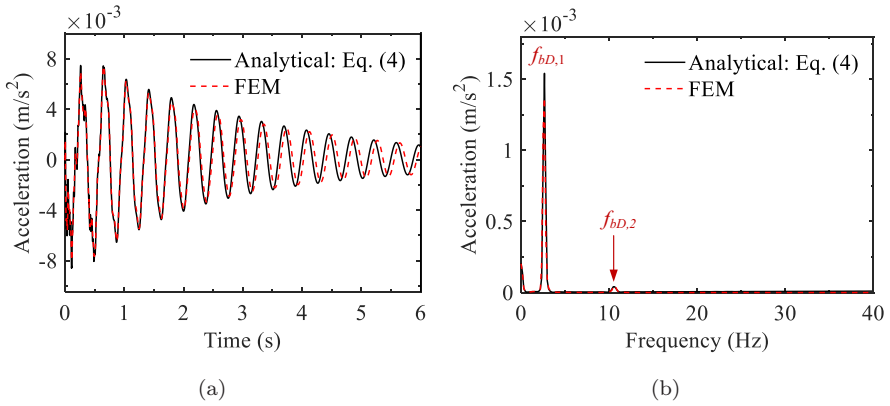|		
Vehicle	Mass	$m_v = 1,000\,\text{kg}$
	Mass moment of inertia	$J_v = 700\,\text{kg} \cdot \text{m}^2$
	Suspension stiffness	$k_{v1} = 550\,\text{kN/m}$
		$k_{v2} = 550\,\text{kN/m}$
	Suspension damping coefficient	$c_{v1} = 2.0\,\text{kN} \cdot \text{s/m}$
		$c_{v2} = 2.0\,\text{kN} \cdot \text{s/m}$
	Axle distance to gravity center	$d_1 = 0.5\,\text{m}$
		$d_2 = 1.5\,\text{m}$
Bridge	Length	$L = 30\,\text{m}$
	Young's modulus	$E = 27.5\,\text{GPa}$
	Moment of inertia	$I = 0.2\,\text{m}^4$
	Mass per unit length	$m = 2,400\,\text{kg/m}$
	Damping ratio	$\xi_b = 2\%$

Fig. 2. Bridge responses: (a) acceleration; (d) spectrum.

and $f_{bD,2} = 10.50\,\text{Hz}$, which coincide quite well with the theoretical ones calculated by Eq. (6b). The slight deviation between the theoretical and FEM results in the rear part responses in Fig. 2(a) is caused by accumulation of errors between the two responses in time domain, which is not equivalent to frequency shift.

4.2. *Verification of back-calculated contact response*

The vehicle's vertical and rotational acceleration spectra calculated by the FEM have been plotted in Figs. 3(a) and 3(b), respectively. On finds that the 1st damped frequency $f_{bD,1}$ ($= 2.67\,\text{Hz}$) of the bridge can be clearly identified, but the 2nd damped frequency $f_{bD,2}$ ($= 10.50\,\text{Hz}$) is only marginally visible. In fact, this is due
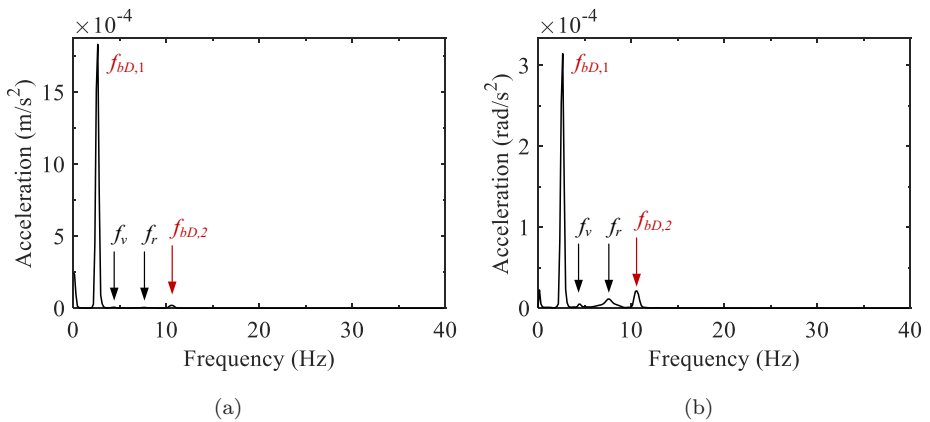

Fig. 3. Vehicle's spectra: (a) vertical acceleration; (b) rotational acceleration.
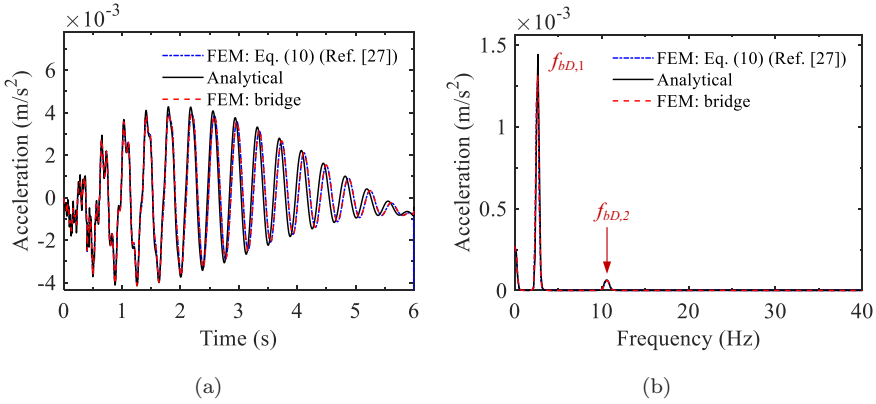
Fig. 4. Front contact responses: (a) acceleration; (b) spectrum.

to the presence of the vehicle's vertical frequency f_v and rotational frequency f_r in the same spectra, which tend to mask the bridge frequencies.

The above masking effect on the bridge frequencies can be circumvented, if the contact responses, rather than vehicle's responses, are used. Since the front and rear contact responses are similar, only the former will be shown herein. To this end, the front contact responses back-calculated analytically from the vehicle's responses using Eq. (10) and the discrete version of Eq. (10)[31] have been plotted in Fig. 4, along with the FEM ones directly obtained from the bridge response. From Fig. 4(b), one finds that the magnitudes of the first two bridge frequencies have been made larger, due to suppression of the vehicle's vertical and rotational frequencies. Aside from this, it is clear that the back-calculated contact responses agree well with the analytical and FEM solutions in both time and frequency domains.

4.3. *Determination of bridge damping ratio*

In this section, the reliability of the formula in Eq. (18) for determining the first bridge damping ratio will be assessed, using the data reported in Secs. 4.1 and 4.2. For the vehicle of length $d = 2.0\,\mathrm{m}$, the instantaneous amplitudes of the 1st component response of the damped bridge for the front and rear contact responses, i.e. $A_{c1}(t)$ and $A_{c2}(t + t_2)$ based on Eq. (16), have been plotted in Fig. 5. By using the correlation between the instantaneous amplitudes of the front and rear contact responses, i.e. Eq. (18), the first damping ratio of the bridge of length $L = 30\,\mathrm{m}$ can be identified, shown as blue dots in Fig. 6, where the abscissa has been selected as location rather than time for better display of the spatial correlation of the front and rear contact points. It should be noted that the blue dots Fig. 6 are just representative points for graphic display. In reality, every data point obtained by Eq. (18) has been used in the calculation. To discard the discontinuity end effect
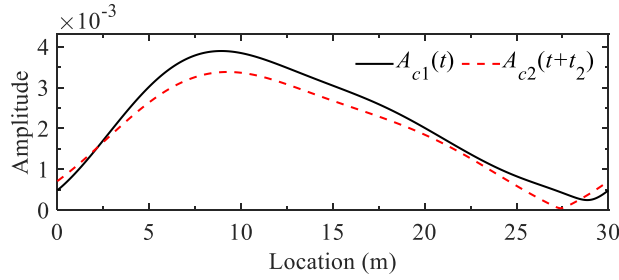
Fig. 5. Instantaneous amplitudes of the 1st component responses of the bridge recovered from the front and rear contact responses.
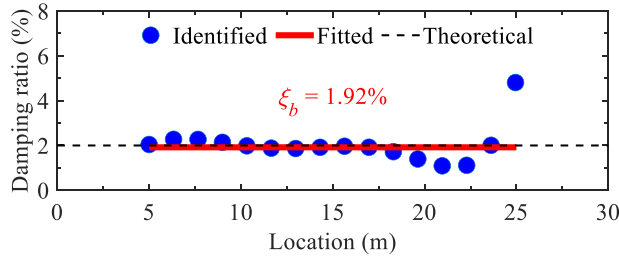

Fig. 6. Identification result of bridge damping ratio.

both physically and by the HT technique, the measured results close to the two ends (5 m) of the bridge are manually abandoned.

Since damping is not likely to vary with bridge location, the fitted slope for the measured results is therefore set to zero, which is obtained as the blue dots in Fig. 6 using the least absolute residuals. The damping ratio so obtained is 1.92% for the 1st mode of the bridge. This value is close to the theoretical value 2% (dashed line in Fig. 6) with an error of 4.00%. As a result, the proposed formula has been demonstrated to be capable of extracting the first damping ratio of the bridge, using the correlation between the two contact points of the two-axle test vehicle.

It should be noted that by nature, damping tends to reduce the amplitudes of bridge responses. For modes other than the first one, the (instantaneous) amplitudes of the component responses may not be large enough for the damping ratios to be identified.

To investigate the applicability of the proposed method for various vehicle speeds, two additional vehicle speeds, i.e. $v = 2.5$ m/s and 10 m/s (9 km/h and 36 km/h), are used, with the results shown in Fig. 7. The identified damping ratios for the two additional vehicle speeds are 1.93% and 2.38%, with errors of 3.50% and 19.00%, respectively. Clearly, to ensure the accuracy of the identified result, the vehicle speed is not recommended to be high.
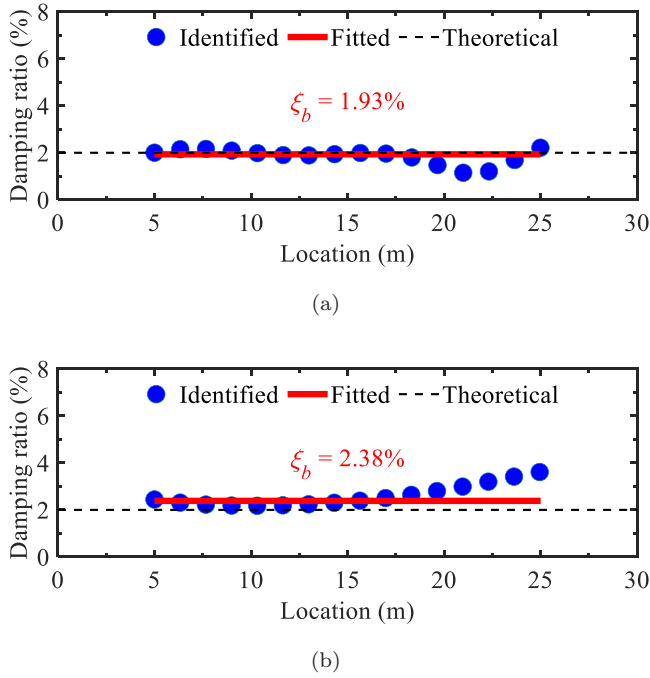
(a)

(b)

Fig. 7. Identification results of bridge damping ratio for various vehicle speeds: (a) $v = 2.5\,\mathrm{m/s}$; (b) $v = 10\,\mathrm{m/s}$.

5. Effect of Pavement Roughness

Pavement roughness is an unfavorable factor in the application of the VSM, which can significantly reduce the quality and accuracy of the scanning technique. In this section, the pavement roughness in Fig. 8 is constructed using the refined roughness formula[34] with class A, which, by taking into account the wheel size effect, is an improved version for the power spectral density (PSD) function of ISO 8608.[35] The effectiveness of the VSM is influenced by the relative amplitudes of bridge vibration and roughness-induced vibration. Undoubtedly, the proposed method is not specifically designed for extreme conditions with high roughness but low bridge vibration. For unfavorable conditions, the method can be enhanced by hardware measures, such as random traffic or extra shaker[25] or by software measures, such as filtering techniques or residual contact response.[4] These technical measures can enhance the signal-to-noise ratio, thereby improving the efficacy of the method.

Previously, existing random traffic has been shown to be capable of magnifying the bridge vibration to the level such that the roughness-induced vibration becomes
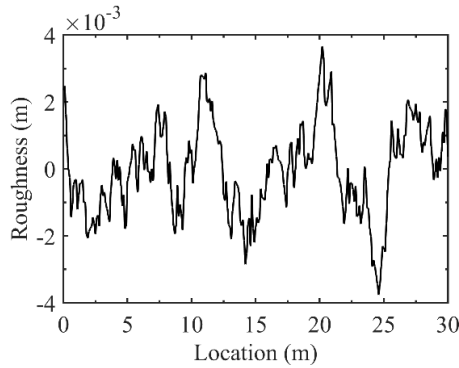
Fig. 8. Pavement roughness.

Table 2. Traffic flow data.

Traffic flow	Car 1	Car 2	Car 3	Car 4
Load (kN)	12.57	14.15	12.54	15.89
Speed (km/h)	51	35	49	47
Entry time (s)	−1.71	1.26	−1.55	1.23

relatively small, thereby enhancing the capability of the VSM.[25] In this study, four additional vehicles will be adopted to simulate the random traffic, of which the loads, speeds, and entry times into the bridge generated randomly by the MATLAB have been listed in Table 2. Each car in Table 2 is modeled as a moving load, neglecting its dynamic interaction with the bridge. In addition, the entry time of the test vehicle into the bridge is set at 0 s. To simulate the bi-directional traffic, Cars 1–2 listed in Table 2 enter the bridge from the same end as the test vehicle, while Cars 3–4 from the other end.

For the circumstance considered, the spectrum of the front contact response has been plotted in Fig. 9. Clearly, the same first two frequencies $f_{bD,1}$ $(= 2.67\,\mathrm{Hz})$ and $f_{bD,2}$ $(= 10.50\,\mathrm{Hz})$ of the bridge can be identified from the spectrum. The first damping ratio identified by the proposed formula for the bridge with rough pavement under random traffic has been plotted in Fig. 10, which yields a damping ratio of $\xi_b = 2.18\%$, with an error of 9%. Since the damping ratio is small in magnitude, a small deviation in identification can lead to a large error. Moreover, due to the random nature of roughness and traffic, the identified result appears to oscillate unpredictably, but around the theoretical value. With this example, the proposed formula has been demonstrated to be capable of detecting the first
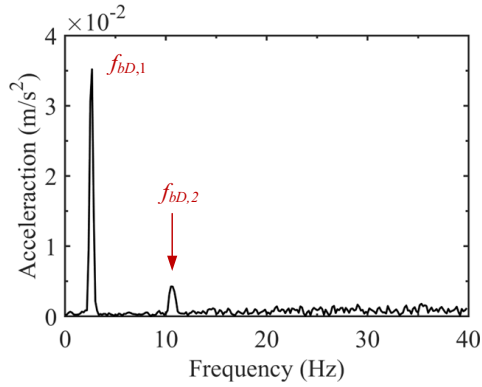
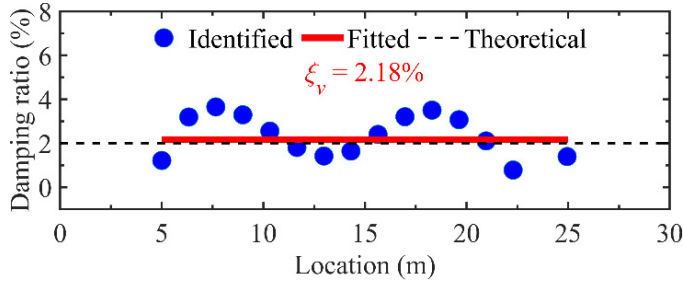Fig. 9. Spectrum of the front contact response.

Fig. 10. Identification result of bridge damping ratio for rough surface under random traffic.

damping ratio of the bridge in the presence of pavement roughness, but with the aid of ongoing traffic.

6. Concluding Remarks

In this paper, a simple formula was derived for determining the bridge damping ratio using the correlation between the instantaneous amplitudes of the related mode of the front and rear contact responses of a two-axle test vehicle by the HT technique. First, closed-form solutions were derived for the dynamic response of the damped bridge and contact points. Then, the damping ratio of the bridge was determined from the correlation of the instantaneous amplitudes of the front and rear contact points of the test vehicle. Based on the theoretical and numerical studies presented herein, it is concluded that the proposed formula can be successfully used for determining the first damping ratio, even for bridges with rough pavement, if use has been made of the "beneficial" excitation by ongoing traffic.

Acknowledgment

ORCID

Y. B. Yang ● https://orcid.org/0000-0003-3149-4966

Y. H. Liu ● https://orcid.org/0009-0000-1590-2697

H. Xu ● https://orcid.org/0000-0003-4786-9021

References

1. R. R. Hou and Y. Xia, Review on the new development of vibration-based damage identification for civil engineering structures: 2010–2019, *J. Sound Vib.* **491** (2020) 115741.
2. S. Das and K. Roy, A State-of-the-art review on FRF-based structural damage detection: development in last two decades and way forward, *Int. J. Struct. Stab. Dyn.* **22**(2) (2022) 2230001.
3. Y. B. Yang, C. W. Lin and J. D.Yau, Extracting bridge frequencies from the dynamic response of a passing vehicle, *J. Sound Vib.* **272** (2004) 471–493.
4. Z. L. Wang, J. P. Yang, K. Shi, H. Xu, F. Q. Qiu and Y. B. Yang, Recent advances in researches on vehicle scanning method for bridges, *Int. J. Struct. Stab. Dyn.* **22**(15) (2022) 2230005.
5. X. Kong, C. S. Cai and B. Kong, Numerically extracting bridge modal properties from dynamic responses of moving vehicle, *J. Eng. Mech.* **142**(6) (2016) 04016025.
6. J. D. Sitton, Y. Zeinali, D. Rajan and B. A. Story, Frequency estimation on two-span continuous bridges using dynamic responses of passing vehicles, *J. Eng. Mech.* **146**(1) (2019) 04019115.
7. H. Xu, C. C. Huang, Z. L. Wang, K. Shi, Y. T. Wu and Y. B. Yang, Damped test vehicle for scanning bridge frequencies: Theory, simulation and experiment, *J. Sound Vib.* **506**(18) (2021) 116155.
8. Y. B. Yang, Y. C. Li and K. C. Chang, Constructing the mode shapes of a bridge from a passing vehicle: A theoretical study, *Smart Struct. Syst.* **13**(5) (2014) 797–819.
9. A. Malekjafarian and E. J. OBrien, Identification of bridge mode shapes using short time frequency domain decomposition of the responses measured in a passing vehicle, *Eng. Struct.* **81** (2014) 386–397.
10. S. S. Eshkevari, T. J. Matarazzo and S. N. Pakzad, Bridge modal identification using acceleration measurements within moving vehicles, *Mech. Syst. Signal Process.* **141** (2020) 106733.
11. X. D. Jian, Y. Xia and L. M. Sun, An indirect method for bridge mode shapes identification based on wavelet analysis, *Struct. Control. Health Monit.* **27**(12) (2020) e2630.
12. A. González, E. J. Obrien and P. J. McGetrick, Identification of damping in a bridge using a moving instrumented vehicle, *J. Sound Vib.* **331** (2012) 4115–4131.

13. J. Keenahan, E. J. OBrien, P. J. McGetrick and A. Gonzalez, The use of a dynamic truck-trailer drive-by system to monitor bridge damping, *Struct. Health Monit.* **13** (2014) 143–157.

14. Y. B. Yang, B. Zhang, Y. N. Chen, Q. Yao and Y. T. Wu, Bridge damping identification by vehicle scanning method, *Eng. Struct.* **183** (2019) 637–645.

15. Y. B. Yang, K. Shi, Z. L. Wang, H. Xu, B. Zhang and Y. T. Wu, Using a single-DOF Test vehicle to simultaneously retrieve the first few frequencies and damping ratios of the bridge, *Int. J. Struct. Stab. Dyn.* **21** (2021) 2150108.

16. Y. B. Yang and K. C. Chang, Extraction of bridge frequencies from the dynamic response of a passing vehicle enhanced by the EMD technique, *J. Sound Vib.* **322** (2009) 718–739.

17. J. P. Yang and W. C. Lee, Damping effect of a passing vehicle for indirectly measuring bridge frequencies by EMD technique, *Int. J. Struct. Stab. Dyn.* **18** (2018) 1850008.

18. W. M. Li, Z. H. Jiang, T. L. Wang and H. P. Zhu, Optimization method based on generalized pattern search algorithm to identify bridge parameters indirectly by a passing vehicle, *J. Sound Vib.* **333** (2014) 364–380.

19. T. Nagayama, A. P. Reksowardojo, D. Su and T. Mizutani, Bridge natural frequency estimation by extracting the common vibration component from the responses of two vehicles, *Eng. Struct.* **150** (2017) 821–829.

20. C. Tan, H. Zhao, E. J. Obrien, N. Uddin and C. W. Kim, Exploring time-varying characteristics in drive-by bridge frequency extraction with the second-order synchrosqueezing transform, *J. Bridge Eng.* **28**(4) (2023) 04023010, doi:10.1061/JBENF2.BEENG-5979.

21. C. Tan, A. Elhattab and N. Uddin, "Drive-by" bridge frequency-based monitoring utilizing wavelet transform, *J. Civil Struct. Health Monit.* **7**(5) (2017) 615–625.

22. Y. Zhan, F. T. K. Au and J. Zhang, Bridge identification and damage detection using contact point response difference of moving vehicle, *Struct. Control Health Monit.* **28**(12) (2021) e2837.

23. J. Li, X.Q. Zhu, S. S. Law and B. Samali, Time-varying characteristics of bridges under the passage of vehicles using synchroextracting transform, *Mech. Syst. Signal Process.* **140** (2020) 106727.

24. H. Wang, T. Nagayama, J. Nakasuka, B. Zhao and D. Su, Extraction of bridge fundamental frequency from estimated vehicle excitation through a particle filter approach, *J. Sound Vib.* **428** (2018) 44–58.

25. H. Xu, Y. H. Liu, M. Yang, D. S. Yang and Y. B. Yang, Scanning and separating vertical and torsional-flexural frequencies of thin-walled girder bridges by a single-axle test vehicle, *Thin-Walled Struct.* **182**(8) (2023) 110266.

26. S. S. Eshkevari, S. N. Pakzad, M. Takác and T. J. Matarazzo, Modal identification of bridges using mobile sensors with sparse vibration data, *J. Eng. Mech.* **146**(4) (2020) 04020011.

27. Q. Mei, N. Shirzad-Ghaleroudkhani, M. Gül, S. F. Ghahari and E. Taciroglu, Bridge mode shape identification using moving vehicles at traffic speeds through non-parametric sparse matrix completion, *Struct. Control Health Monit.* **28**(7) (2021) e2747.

28. J. Li, X. Q. Zhu and J. Guo, Enhanced drive-by bridge modal identification via dual Kalman filter and singular spectrum analysis, *Struct. Control. Health Monit.* **29**(5) (2022) e2927.

29. L. Frýba, *Vibration of Solids and Structures Under Moving Loads* (Noordhoff International Publishing, Groningen, 1972).
30. J. M. Biggs, *Introduction to Structural Dynamics*, (McGraw-Hill, New York, 1964).
31. Y. B. Yang, H. Xu, Z. L. Wang and K. Shi, Using vehicle-bridge contact spectra and residue to scan bridge's modal properties with vehicle frequencies and road roughness eliminated, *Struct. Control Health Monit.* **29**(8) (2022) e2968.
32. C. W. Lin and Y. B. Yang, Use of a passing vehicle to scan the fundamental bridge frequencies - an experimental verification, *Eng. Struct.* **27**(13) (2005) 1865–1878.
33. F. W. King, *Hilbert Transforms: Encyclopedia of Mathematics and its Applications* (Cambridge University Press, Cambridge 2009).
34. H. Xu, M. H. Wang, Z. L. Wang, D. S. Yang, Y. H. Liu and Y. B. Yang. Generation of surface roughness profiles for inclusion in vehicle–bridge interaction analysis and test application, *Int. J. Struct. Stab. Dyn.* **23**(8) (2022) 2350094, doi:10.1142/S0219455423500943.
35. ISO 8680, *Mechanical Vibration-Road Surface Profiles-Reporting of Measured Data* (International Organization for Standardization, Geneva, 1995).